JMES The International Journal of Mechanical Engineering and Sciences
http://iptek.its.ac.id/index.php/jmes/index

Influence of Nozzle-to-Surface Distance Ratio and Reynolds Number Variation on Hemispherical Tempered Glass Strength and Quench Time

Frans Loekito, Budi U.K. Widodo*, and Djatmiko Ichsani

Department of Mechanical Engineering, Institut Teknologi Sepuluh Nopember, Surabaya 60111, Indonesia

Received: 1 January 2017, Revised:8 February 2017, Accepted: 15 March 2017

Abstract

The quench step in a glass tempering process is a transient heat transfer phenomenon which is governed by several parameters – Reynolds number (Re) and the nozzle diameter-to-surface distace ratio (H/D). In this research, the effect of such parameters on the strength and quench time of hemispherical tempered glass are to be analyzed. The quench process will use the impinging jets quench method, with an equilateral – staggered nozzle arrangements. The process is performed in an ambient air of 60°C and with a nozzle pitch and diameter of 27 mm and 4 mm respectively. The study applies variations of Reynolds number: 2300, 10000, 20000, 30000, 40000, 50000, 60000, 70000, 80000, and 87000, and H/D: 2, 6, 9, and 12. These variations are used to construct and solve a mathematical model, to obtain temperature distribution contours. The contours are then transformed into stress distribution graphs. From these steps, it is found that the tempered glass strength increases and the quench time decreases along with the increase of Re and the decrease of H/D. It is also found that the allowable range of operation is between Re=8000 – 25000 for H/D =2 and Re = 8000 – 30000 for H/D = 6, 9, and 12.

Keywords: Impinging jet, Quenching, Tempered glass, Transient conduction.

1. Introduction

Commercial glasses, based on their manufacturing process, are differentiated into two groups: annealed glass and tempered glass. By administering a four-point-bending test (ASTM 1161-13) [1] it is universally known that annealed glass has a high allowable compression strength and hardness. However, this type of glass is also notorious for its low tensile strength. To cope with this weakness, a glass strengthening method, which produce tempered glass – a type of glass having a tensile strength about five times higher than annealed glass – is then developed [2]. Hemispherical tempered glass manufacturing processes is done in two steps: heating and quenching (Figure 1). During the heating process, the glass must be heated uniformly between the softening point (712°C) and the transition point (560°C). In the quenching step, the glass is rapidly cooled until its temperature falls below the strain point (510°C). In the quenching process, there are some control parameters, namely the initial temperature, glass geometry, and quench rate [2, 3].

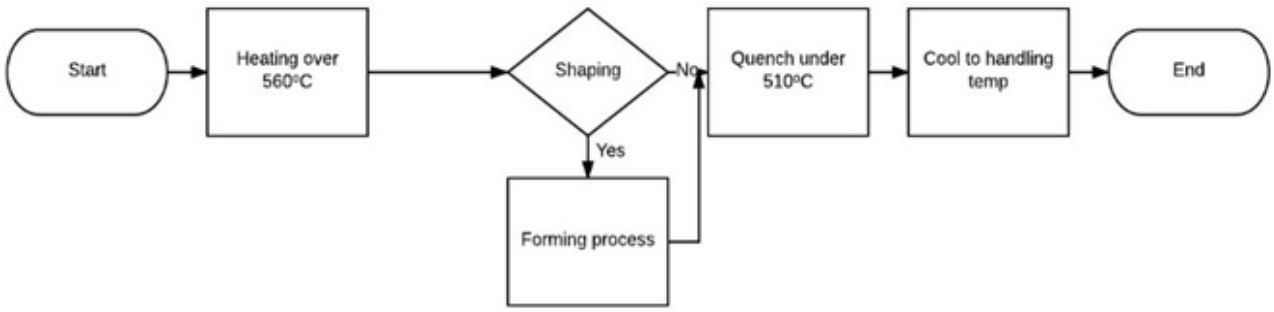

Figure 1. Glass tempering process' flowchart.

*Email:buditem@me.its.ac.id
Phone:+6281553843834

Over several decades, theories regarding effect on convection coefficient and the tempered glass strength has been developed by Gardon (1965) and Sinha (1978). Gardon's study revealed that the glass strength will increase with a rise in quench rate. This increase, however, comes with an additional restriction on the operational parameters: an increase in the convection coefficient will also increase the lowest allowable initial quenching temperature [4]. Sinha's theory complements Gardon's experimental approach by proposing an equation to determine the tempered glass local internal stresses (σ_x) based on its local temperatures,T_x (Equation 1) [5]

$$\sigma_x(t) = \frac{\varepsilon\alpha}{1-v}(T_x(x) - T_{avrg}(t)) \quad (1)$$

where E, α, and are the glass elasticity, coefficient of linear thermal expansion, and Poisson's ratio, respectively. To relate the glass strength values with standards in industrial applications, Rajan (2005) correlate the glass midplane tension (σ_m) with the local strain energy, which is used to calculate the glass fragment size, x (Equation 2) [6].

$$x = 2(1-v)\left(\frac{K_{1C}}{\sigma}\right)^2 \frac{t}{t-2\delta} \quad (2)$$

K_{1c} is described as the glass surface toughness, while t and δ are the glass thickness and the tempered glass compression layer thickness, respectively. Supported by these previous works, this study aims to investigate the effect of nozzle-to-surface distance ratio and Reynolds number on hemispherical tempered glass strength.

2. Methods

2.1. Glass and Nozzle Dimension

The model used in this study is a hemispherical soda lime glass with dimension as shown in Table 1.The nozzle arrangement used in this study is a horizontal equilaterally staggered round nozzles with dimension as shown in Table 1 and Figure 2.

Table 1. Glass and nozzle dimension

Parameter	Size
Nozzle Diameter (nozzle)	4 mm
Radius Dome (Rdome)	622.56 mm
Hemisphere Diameter (hemisphere)	400 mm
Diagonal Nozzle Pitch (Pd)	27 mm
Transverse Nozzle Pitch (Pt)	27 mm
Total Nozzle	190

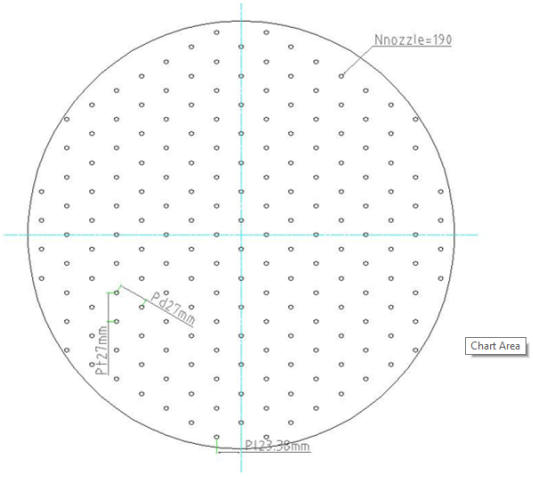

Figure 2. Top view of the nozzle arrangement.

2.2. Meshing and Boundaries

The mathematical model will be a 2D transient conduction in polar coordinates approach, which uses a radial quadrilateral-map type of mesh for the glass, with 4θ nodes in the r-direction and 2θ nodes in the θ -direction. The boundary conditions for the glass consist of convection on both surfaces, with an initial temperature of 625° C (Figure 3).

Table 2. Fluid and glass mechanical and thermal properties

Parameter		Input
Fluid	Air	Tf = 60°C ρ = 1.08 kg/m3 μ = 196.4 x 10^{-7} N.s/m kf = 0.028 W/m.K Pr = 0.7035 Cp = 1.008 kJ/kg.K
Glass	Soda lime glass	E = 7.45 x 1010 N/m2 v = 0.201 a = 7.7 x 10^{-6} /K k = 0.8793 W/m.K K_{1c} = 2.15 Mpa/m0.5

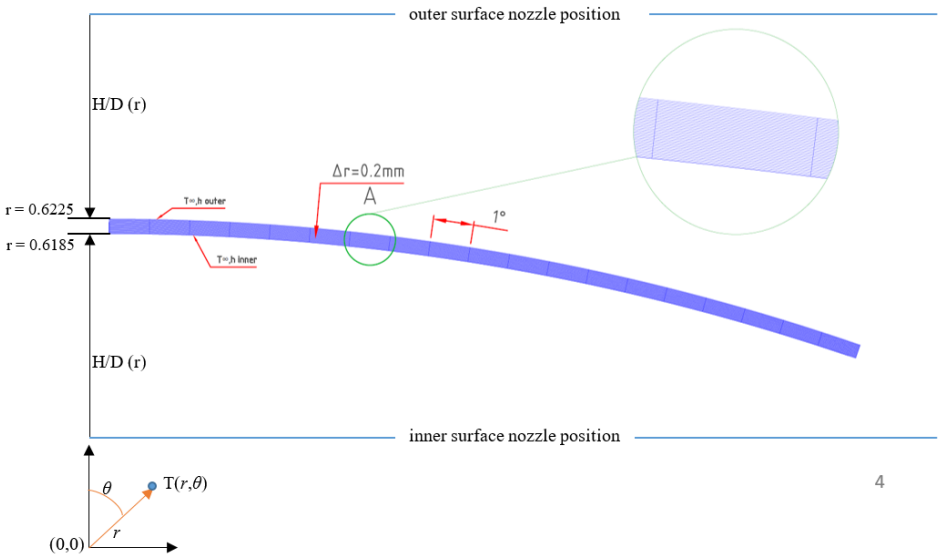

Figure 3. Glass meshing and boundary condition.

2.3. Convection Coefficient Calculation

The convection coefficient for each node is calculated using impinging jet with an array of round nozzle on a flat surface (Equation 3,4,5,6) [7].

$$\frac{Nu}{Pr^{0.42}} = 0.5KGRe^{2/3} \tag{3}$$

$$G = 2A_r^{0.5}\frac{1-2.2A_r^{0.5}}{1+0.2\left(\frac{H}{D}-6\right)A_r^{0.5}} \tag{4}$$

$$K = \left[1+\left(\frac{fracHD}{\frac{0.6}{A_r^{0.5}}}\right)^6\right]^{-0.05} \tag{5}$$

$$h = \frac{Nukf}{\phi_{nozzle}} \tag{6}$$

Ar, the relative nozzle area, is defined as the ratio between the nozzle exit area and each nozzle's average impingement area Figure 4. For an equilateral staggered nozzle, Ar can be written as (Equation 7).

$$A_r = \frac{\pi D_{nozzle}^2}{2\sqrt{3}s^2} \tag{7}$$

where s is the nozzle pitch (S = Pd (diagonal pitch) = Pt (transverse pitch)). In this research, both the inner and outer surface H/D at $\theta = \theta_0$ is varied at 2, 6, 9 and 12. However, due to the surface curvature, Equation 3-7 will be used to calculate Nu at every θ (Figure 5, with H/D value at $\theta \neq \theta_0$ will differ according to geometrical consideration (sphere). Equation 8 for the outer surface and Equation 9) for inner surface.

$$\frac{H}{D}(\theta) = \frac{H+0.6225-0.6225cos\theta}{d_{nozzle}} \tag{8}$$

$$\frac{H}{D}(\theta) = \frac{H-0.6225+0.6225cos\theta}{d_{nozzle}} \tag{9}$$

Additionally, the Reynolds number variations will be Re = 2300, 10000, 20000, 30000, 40000, 50000, 60000, 70000, 80000, 87000. The fluid's properties can be seen on Table 2.

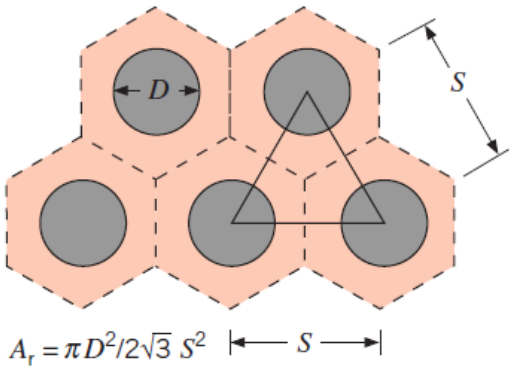

Figure 4. Plan view of geometrical features for equilateral staggered array of round jets.

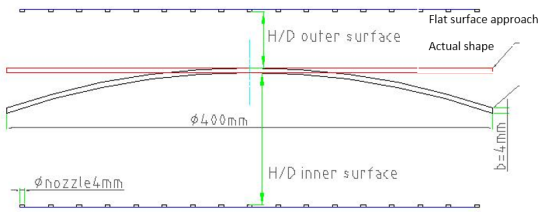

Figure 5. Impinging jet with an array of round nozzle on a flat surface approach.

2.4. Mathematical Modelling and Solving

The transient conduction's parabolic equation (Equation 10) is differentiated using an implicit scheme with forward difference approximation with respect to time increment and central difference approximation with respect to space increment [8].

2.5. Calculation of Local Stresses and Fracture Size

The solutions of the parabolic equations represent the glass' temperatures after all local temperatures is below strain point (510°C) [2, 3]. They are then calculated using (Equation 1) to determine the surface compression (τc; r = 0.6185 mm or r = 0.6225, whichever is lower) and midplane tension (τt). The glass' properties are as seen in Table 2. Each variation's midplane tension is used in accordance with (Equation 2) to calculate its fragment size (x). The resulting size is then compared to ECE R43 standard [9].

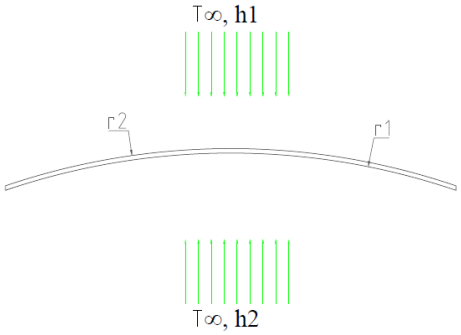

Figure 6. Convection boundary conditions.

$$\frac{1}{r^2}\frac{\partial}{\partial r}\left(kr^2\frac{\partial T}{\partial r}\right)+\frac{1}{r^2 sin^2\theta}\frac{\partial}{\partial \phi}\left(k\frac{\partial T}{\partial \phi}\right)+\frac{1}{r^2 sin\theta}\frac{\partial}{\partial \theta}\left(ksin\theta\frac{\partial T}{\partial \theta}\right)+q=\rho C_p\frac{\partial T}{\partial t} \tag{10}$$

$$T_{i,j}^{n}=\left(2\Delta t\alpha\left(\frac{1}{(r\Delta\theta)^2}+\frac{1}{\Delta r^2}\right)+1\right)T_{i,j}^{n+1}-\frac{\alpha\Delta t}{\Delta r}\left(\frac{1}{\Delta r}+\frac{1}{r}\right)T_{i+1,j}^{n+1}-\frac{\alpha\Delta t}{\Delta r}\left(\frac{1}{\Delta r}+\frac{1}{r}\right)T_{i-1,j}^{n+1}-$$
$$\frac{\alpha\Delta t}{r\Delta\theta}\left(\frac{1}{r\Delta\theta}+\frac{ctg\theta}{2r}\right)T_{i,j+1}^{n+1}-\frac{\alpha\Delta t}{r\Delta\theta}\left(\frac{1}{r\Delta\theta}+\frac{ctg\theta}{2r}\right)T_{i,j-1}^{n+1} \tag{11}$$

$$T_{i,j}^{n}+\frac{2h_2\alpha\Delta t}{k}\left(\frac{1}{\Delta r}+\frac{1}{r}\right)T_f=\left(2\Delta t\alpha\left(\frac{h_2}{k\Delta r}+\frac{h_2}{r}+\frac{1}{(r\Delta\theta)^2}+\frac{1}{\Delta r^2}\right)+1\right)T_{i,j}^{n+1}-\frac{2\alpha\Delta t}{\Delta r}T_{i+1,j}^{n+1}-$$
$$\frac{\alpha\Delta t}{r\Delta\theta}\left(\frac{1}{r\Delta\theta}+\frac{ctg\theta}{2r}\right)T_{i,j+1}^{n+1}-\frac{\alpha\Delta t}{r\Delta\theta}\left(\frac{1}{r\Delta\theta}+\frac{ctg\theta}{2r}\right)T_{i,j-1}^{n+1} \tag{12}$$

$$T_{i,j}^{n}+\frac{2h_2\alpha\Delta t}{k}\left(\frac{1}{\Delta r}+\frac{1}{r}\right)T_f=\left(2\Delta t\alpha\left(\frac{h_2}{k\Delta r}+\frac{h_2}{r}+\frac{1}{(r\Delta\theta)^2}+\frac{1}{\Delta r^2}\right)+1\right)T_{i,j}^{n+1}-$$
$$\frac{2\alpha\Delta t}{\Delta r}T_{i+1,j}^{n+1}-\frac{\alpha\Delta t}{r\Delta\theta}\left(\frac{1}{r\Delta\theta}+\frac{ctg\theta}{2r}\right)T_{i,j+1}^{n+1}-\frac{\alpha\Delta t}{r\Delta\theta}\left(\frac{1}{r\Delta\theta}+\frac{ctg\theta}{2r}\right)T_{i,j-1}^{n+1} \tag{13}$$

3. Results and Discussion

3.1. Qualitative Analysis on the Temperature Contours

The result of MATLAB simulation of previous parabolic differential equations is displayed in a temperature contour, such as Figure 7 (Re = 60000, H/D = 9). As seen in the figure, while the both surfaces have the overall lowest temperatures, the outer surface (r = 0.6225) has higher temperatures than the inner surface (r = 0.6185). It can also be noted from Figure 8 that while in the outer surface, θ = 19°C has a higher temperature than θ=θ_0, the trend is inverted for the inner surface. Both disparities were due to the glass' curvature, as a larger gap between the nozzles and the surface will cause a decrease in convection coefficient, which in turn will increase the resulting local temperature [7]. From Figure 7, it can also be seen that after a certain time, the glass interior temperatures will be below the glass' strain point (783 K), which in this case is t = 5.25 s. In this study, this value of time will further be called as the glass quench time (tq). Based on quench time, the variations in this study are classified into five groups, as shown by the Table 3. The comparison between each group's temperature contours can be seen on Figure 9. In this figure, the contours are taken after the glass has been quenched for 5 seconds. Group A's local temperatures have fallen well beneath the strain point while Group B's midplane local temperatures are approximately similar to that of strain point, hence it can be said that both Group A and B have reached their respective quench time. On the other hand, Group C, D, and E have local midplane temperatures higher than the strain point, which shows that all three groups have not yet reach their quench time.

Figure 7. Glass temperature contour during quench with Re = 60000 and H/D = 9.

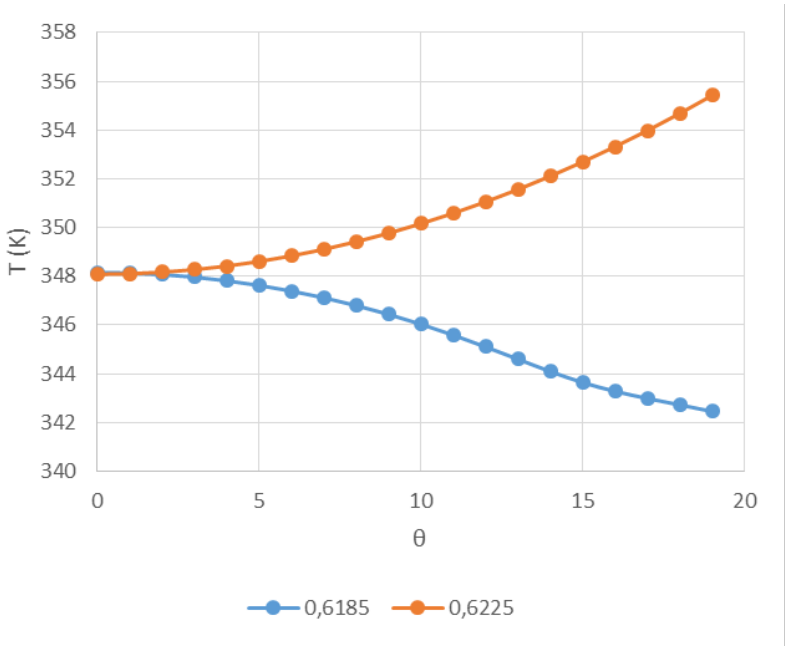

Figure 8. Inner and outer surface temperature graph during quench with Re = 60000 and H/D = 9, t = 5s.

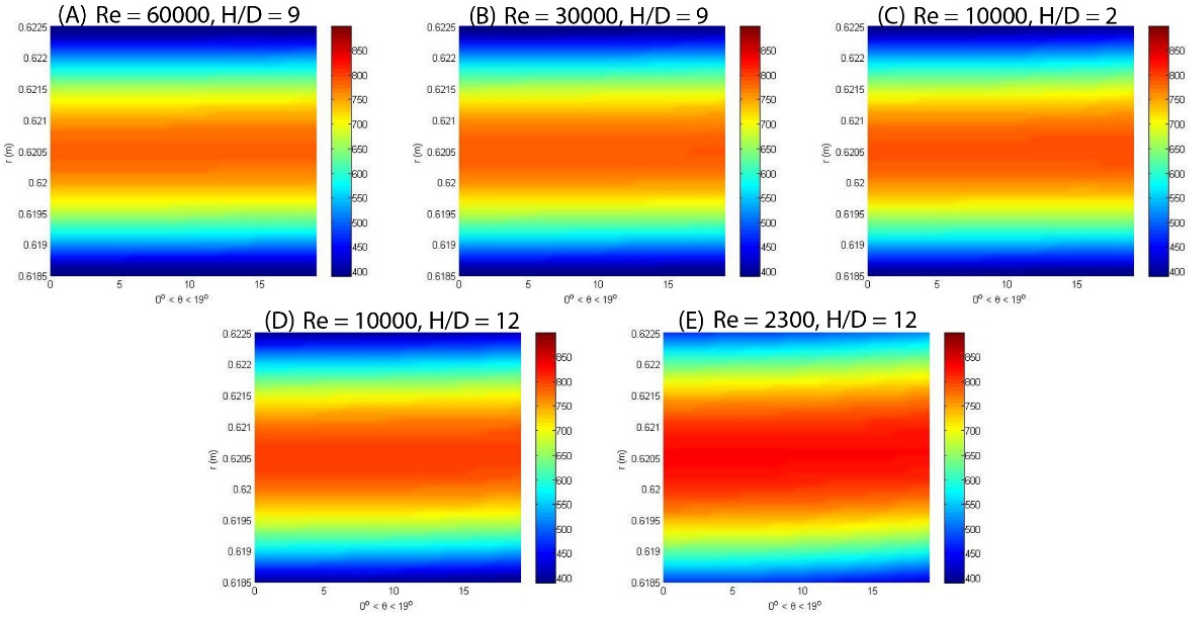

Figure 9. Comparison between temperature contours of all five groups after the glass has been quenched for 5 seconds.

Figure 9 also introduces another intriguing pattern. By comparing the contours of Group C and D, it is obvious that the overall temperature, especially the midplane local temperatures, of a glass quenched in lower H/D value will be higher than that quenched in higher H/D value. Conversely, an increase in Reynolds number produce a lower midplane local temperatures and the glass overall temperature. This claim is plausible, considering the congruity between this trend and the effect of both H/D and Re value implied by Equation 3-6 [7]. Additionally, by comparing Group D and E, it can be concluded that a higher Re will also yield a more uniform surface

Table 3. Classification of each variation based on its quench time

Group	Quench time (s)	H/D	Re
A	t 5.3	2	Re = 30000 – Re = 87000
		6	Re = 40000 – Re = 87000
		9	Re = 50000 – Re = 87000
		12	Re = 60000 – Re = 87000
B	5.3< t 5.5	2	Re = 20000
		6	Re = 20000 – Re = 30000
		9	Re = 20000 – Re = 40000
		12	Re = 30000 – Re = 50000
C	5.5< t 5.6	2	Re = 10000
		12	Re = 20000
D	5.6< t 5.8	2	Re = 10000
		6	Re = 10000
		9	Re = 10000
		12	Re = 10000
E	t > 5.8	2	Re = 2300
		6	Re = 2300
		9	Re = 2300
		12	Re = 2300

temperature distribution.

3.2. Stress Distribution Analysis

The glass temperature contours for each variation's quench time is then converted into stress distribution graphs using Equation 1 [5]. As displayed by Figure 10, the stress distribution graph produced by hemispherical tempered glass exhibits a parabolic tendency, similar to that of flat tempered glass. However, the glass' curvature introduces an interesting effect on the graph: a disparity between the glass two surfaces' compression stress values. The outer surface (r_o) has an overall lower compression stress than the inner surface (r_i). Furthermore, the local stress of each surface has a contrasting trend; higher value of θ on the inner surface have a higher compression stress value, while inversely, higher value of θ on the outer surface have a lower compression stress value. Indeed, these observations are justified as it fit the previous claim of higher local temperatures on the outer surface. The nuanced compression stress between each θ can also be correlated with the varying surface's local temperatures. However, if compared to the stress distribution graph of a higher Re (Figure 11), the dissimilarities in the trend are palpable. A higher Re will produce a higher value of both surface compression and midplane tension. This trend is valid, as a higher Re will produce a lower glass average temperature and thus increase the local stresses (Eq 1) [5]. Furthermore, similar to the aforementioned temperature contour tendency in Figure 9, a higher Re also produces a more uniform stress distribution graph.

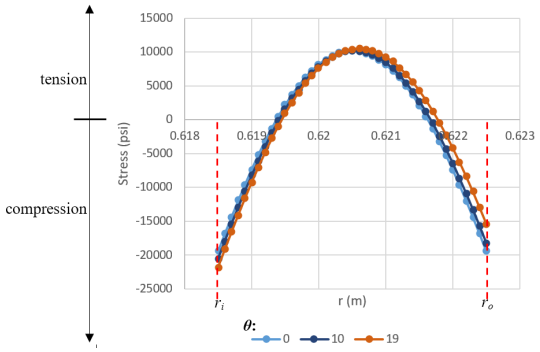

Figure 10. Stress distribution graph of glass quenched in Re=2300, H/D = 6, tq = 6.55s.

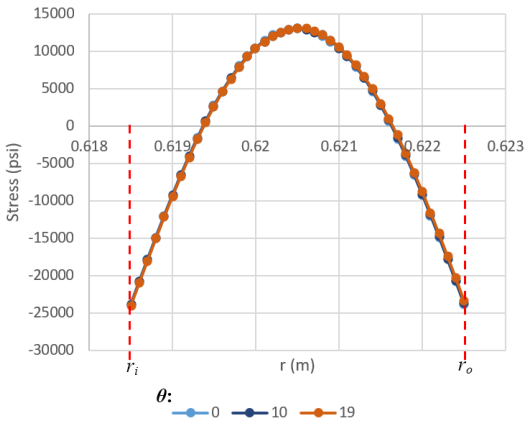

Figure 11. Stress distribution graph of glass quenched in Re=87000, H/D = 6, tq = 5.2 s.

$$\sigma_{sfc} = \begin{cases} 3664.43Re^{0.198} \cdot \left(\frac{H}{D}\right)^{-0.065}, [Re \leq 8000] \\ 43167.84Re \cdot \left(\frac{H}{D}\right)^{-0.006156} - 35872.24, [8000 \leq Re \leq 30000] \\ 3664.43Re^{0.0204} \cdot \left(\frac{H}{D}\right)^{-0.005} - 20099.83, [Re \leq 30000] \end{cases} \quad (14)$$

$$\sigma_q = \begin{cases} 16.078 \quad Re^{-0.12} \cdot \left(\frac{H}{D}\right)^{0.028}, [Re \quad \leq \quad 6500] \\ 8.08Re^{-0.04} \cdot \left(\frac{H}{D}\right)^{0.005}, [Re \quad \geq \quad 6500] \end{cases} \quad (15)$$

3.3. Effect of Re and H/D Values on Surface Compression

After each variation's surface compression value has been calculated, a graph containing all surface compression (σ_{sfc}) values is the constructed (Figure 12). From the above figure, the value of σ_{sfc} converges on higher Re– the effect on both H/D and Re values diminished on higher Re. Based on this inclination, the graph can be divided into three regions: region 1 (Re 8000), region 2 (8000 Re 30000), and region 3 (Re 30000). The proposed correlation for the graph is calculated using LABFIT software [10], which yields:

The outer surface compression value based on the proposed correlation for each region is also available on Figure 12. These correlations have an R-squared value of 95% [10]. Comparison between the three correlations can show the actual effect of Re and H/D values on σ_{sfc} in each region. In region 1, where the power of ReandH/D is the highest, variations in both Re and H/D values cause a great shift in σ_{sfc}. Conversely, in region 2, where the power of Re and H/D is lower than region 1, the value of σ_{sfc} is affected less by change in Re and H/D, and so on.

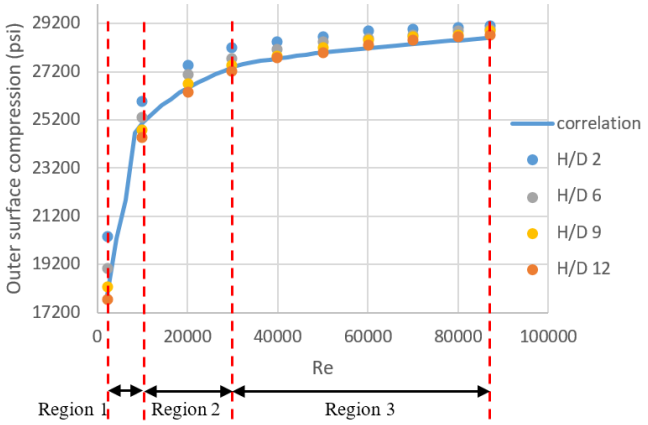

Figure 12. Outer surface compression graph with respect to Re and H/D and its proposed correlation (H/D = 12).

3.4. Effect of Re and H/D Values on Quench Time

Similarly, each variation's quench time can also be assembled into a graph (Figure 13). The figure also shows a converging value of t_q on higher Re. This trend enables division of the graph into two regions: region 1 (Re 6500) and region 2 (6500). Using LABFIT [10], the proposed equation for the graph can be written as:

These correlation's fit on the data can be seen on Figure 11. The correlations have an R-squared value of 92% [10]. Comparison between the two correlations can show the actual effect of Re and H/D values on tq in each region. In region 1, where the power of Re and H/D is the highest, variations in both Re and H/D values cause a great shift in t_q. Conversely, in region 2, where the power of Re and H/D is lower than region 1, the value of t_q is affected less by change in Re and H/D.

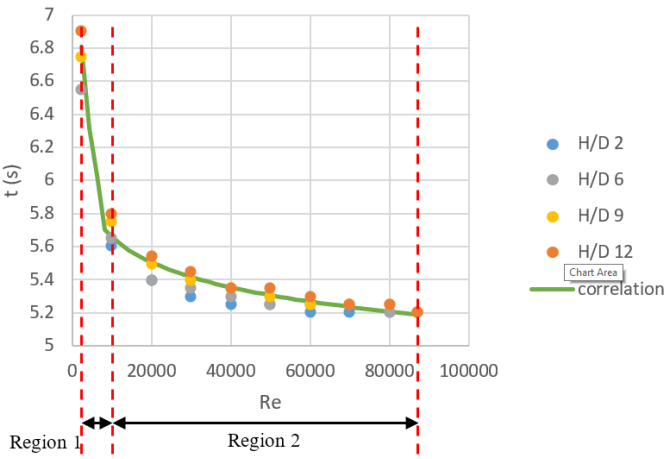

Figure 13. Quench time graph with respect to Re and H/D and its proposed correlation (H/D = 12).

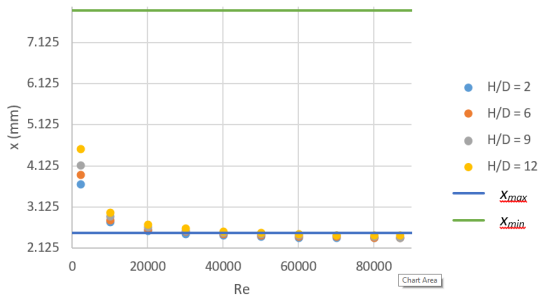

Figure 14. Each variation's fragment size and ECE R43 specification limit.

3.5. Operation Limit Determination Based on ECE R43 Standard

After the effect of Re and H/D valued on both σ_{sfc} and t_q is identified, the optimal range of the two parameters is then determined. Based on European Standard ECE R43, the maximum and minimum allowable number

of fragments for a 50 mm x 50 mm tempered glass is 400 and 40 respectively [9]. Simple mathematic calculation is used to convert the value into minimum and maximum fragment size (x; xmin = 2.5 mm and xmax = 7.9 mm). Each variation's midplane tension is then calculated by Equation 2 to yield its fragment size. The list of each variation's fragment size can be seen on Table 4 and Figure 14. Based on this figure, it is implied that an increase in Re will decrease x. Similarly, a decrease in H/D will also increase x. This is a reasonable conclusion, as the glass' midplane tension, which determines the fragment size, exhibits similar behavior. Based on the figure and the table, it is also shown that all variations' fragment sizes are well below the maximum allowable fragment size (xmax). However, some variations produce fragments smaller than the minimum allowable fragment size (xmin), as is exhibited in the red cells part of Table 4. Hence, the allowable range based on ECE R43 standard is Re = 2300 – 2500 for H/D = 2, Re = 2300 – 31000 for H/D= 6, Re = 2300 – 36000 for H/D = 9, and Re = 2300 – 50000 for H/D = 12. Based on previous discussion regarding Re and H/D effect on σ_{sfc} and tq it is shown that the values of both Re and H/D is more crucial for σ_{sfc} than for t_q. For an optimum operation condition, the value of σ_{sfc} produced must high stability (does not easily experience any steep changes), as well as considerable flexibility (able to yield significant change in value if desired). Therefore, it is safe to decide that Re = 8000 – 30000 (region 2 forσ_{sfc}) as the desired operation range. This conclusion does not consider the fact that the proposed Re values are located in region 2 of the tq graph, as a difference of 0.4 s – the maximum discrepancy between tq ofRe = 6500 and Re = 30000 – will not bring a salient setback in the manufacturing process The desired operation range (Re = 8000 – 30000) is then combined with fragment size calculation result. As some of the proposed range is beneath violate the specifications required by ECE R43 standard, the range must be adjusted for each H/D variation. The resulting allowablw ranges are: Re = 8000 – 25000 for H/D = 2 andRe = 8000 – 30000 for H/D = 6, 9, and 12.

Table 4. Each variation's fragment size (in mm)

Re\ H/D	2	6	9	12
2300	3,659	3,912	4,135	4,541
10000	2,744	2,820	2,895	2,995
20000	2,556	2,590	2,646	2,708
30000	2,469	2,519	2,556	2,606
40000	2,431	2,475	2,498	2,522
50000	2,411	2,434	2,464	2,507
60000	2,391	2,415	2,431	2,470
70000	2,385	2,411	2,424	2,440
80000	2,382	2,387	2,416	2,434
87000	2,372	2,382	2,393	2,423

4. Conclusions

1. From the temperature contour, it can be concluded that:
   (a) A low Re will yield an overall higher glass temperature, and vice versa.
   (b) A low H/D will yield an overall lower glass temperature, andvice versa.
2. From the stress distribution graph, it can be concluded that:
   (a) The stress distribution graph is parabolic.
   (b) A high Re will produce a more uniform surface compression.
   (c) A low Re will cause a nuanced value on each θ surface compression.
3. Based on the comparison of each variations' surface compression and quench time, it can be concluded that:
   (a) σ_{sfc} and t_q values will converge on high Re
   (b) Re andH/D have the highest effect to σ_{sfc} in 2300 Re 8000, moderate effect in 8000 Re 30000, and the lowest effect in Re 30000.
   (c) Re and H/D have the highest effect to tq in Re 6500 and the lowest in Re 6500.
   (d) The correlation between Re, H/D, and σ_{sfc} is given in Equation 14.
   (e) The correlation betweenRe, H/D, and t_q is as Equation 15.
   (f) From both correlation, in accordance with ECE R43 standard, it is concluded that the allowable parameter's ranges are: Re = 8000 – 25000 for H/D = 2 and Re = 8000 – 30000 for H/D = 6, 9, and 12.

References

[1] A. C1161-13, *The Glass Tempering Handbook: Understanding the Glass Tempering Process*, ch. The Glass Tempering Handbook: Understanding the Glass Tempering Process. ASTM International, West Conshohocken, PA, 2013.

[2] R. Gardon, "Thermal tempering of glass," *Glass: Science and technology*, vol. 5, pp. 145–216, 1980.

[3] J. Barr, *The Glass Tempering Handbook: Understanding the Glass Tempering Process*. Self publishing.

[4] R. Gardon, "The tempering of flat glass by forced convection," *Proc. Int. Congr. Glastt, 7th, Institut. National du Verre, Charleroi, Belgique*, 1965.

[5] N. K. Sinha, "Stress state in tempered glass plate and determination of heat-transfer rate," *Experimental Mechanics*, vol. 18, no. 1, pp. 25–34, 1978.

[6] R. Tandon and S. J. Glass, "Controlling the fragmentation behavior of stressed glass," in *Fracture Mechanics of Ceramics*, pp. 77–91, Springer, 2005.

[7] F. Incropera and D. DeWitt, *Introduction to Heat Transfer*. Wiley, 7 ed., 2012.

[8] S. Chapra and R. Canale, *Numerical Methods for Engineers*. Mc Graw-Hill Companies. Inc, 2010.

[9] UNEC, "Uniform provisions concerning the approval of safety glazing materials and their installation on vehicles," tech. rep., United Nations Economic Commission for Europe, 2012.

[10] W. Silva and C. Silva, "Lab fit curve fitting software (nonlinear regression and treatment of data program)," *V*, vol. 7, no. 36, pp. 1999–2007, 1999.